J. Plasma Fusion Res. Vol.102, No.5 (2026) 198-202

小特集 逆磁場ピンチ研究がもたらしたもの

5. Micro-Turbulence in Reversed-Field Pinch Plasmas with Improved Confinement Due to Current Drive

NISHIZAWA Takashi[1)], PUESCHEL M.J.[2,3,4)] and KOSUGA Yusuke[1)]

[1)]Kyushu University, [2)]Dutch Institute for Fundamental Energy Research, [3)]Eindhoven University of Technology, [4)]Ruhr University Bochum

(原稿受付：2025 年 12 月 13 日)

Reversed-field pinches (RFPs) have a unique magnetic field configuration: the strength of the poloidal field is comparable to that of the toroidal field, and the direction of the toroidal field reverses its sign as one moves from the core to the edge. In standard RFP discharges, multiple tearing modes are destabilized on closely-spaced rational surfaces that overlap, creating stochastic magnetic fields. However, by utilizing an inductive current profile control technique called pulsed poloidal current drive (PPCD), the tearing modes can be stabilized, and largely-intact nested flux surfaces can be sustained in an RFP. In such plasmas, micro-turbulence plays an important role in transport, similar to tokamaks and optimized stellarators, and thus micro-instabilities and their nonlinear behavior require study in this less-explored parameter regime. This article reviews both theoretical and experimental investigations of micro-turbulence in RFP discharges with the application of PPCD.

Keywords:
reversed-field pinch, micro-turbulence, trapped-electron mode, zonal flow, gyrokinetic simulation

5.1 Introduction

Historically, comparatively little attention has been paid to micro-instabilities in reversed-field pinches (RFPs), since the stochastic magnetic fields resulting from tearing instabilities tend to govern the heat and particle transport in such devices.

However, drift-wave-like fluctuations have been experimentally observed at high wave numbers in an RFP's stochastic field [1]. The turbulent kinetic energy of these modes is much smaller than that originating from tearing modes, and thus, the transport is still thought to be determined primarily by tearing-mode activity. As measures through which nested flux surfaces are restored in RFP plasmas, *i.e.*, pulsed poloidal current drive (PPCD) and quasi-single helicity (QSH) scenarios, have been developed, micro-instabilities in the RFP has become the subject of active research. The details of these operations of RFP plasmas are discussed in Refs. [2, 3]. In QSH, one tearing mode grows to a large amplitude while the amplitudes of other tearing modes are reduced, leading to nested helical flux surfaces in the core, reminiscent of a stellarator. Reference [4] investigated micro-instabilities in this state and found that microtearing modes can become unstable. Conversely, PPCD weakens tearing modes at all mode numbers by disrupting the dynamo effect with poloidal inductive currents, restoring axi-symmetric flux surfaces. Flux surfaces and field lines in a typical RFP plasma with PPCD are shown in Fig. 1(a). While axisymmetric, this magnetic configuration is distinct from those of tokamaks. The pitch of the magnetic fields is often characterized by the safety factor q, which indicates how many times a magnetic field line travels toroidally to complete one poloidal loop. The radial q profile in an RFP plasma is depicted in Fig. 1(b).

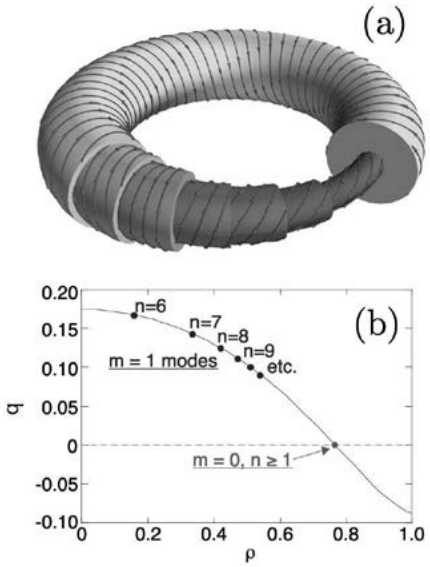

Fig. 1 Flux surfaces and field lines in an RFP discharge with PPCD (a) and the corresponding safety factor profile as a function of radial coordinate ρ (b). Due to the low safety factor, many rational surfaces exist, and tearing modes become unstable without PPCD.

Research Institute for Applied Mechanics, Kyushu University, Kasuga, FUKUOKA 816-8580, Japan
corresponding author's e-mail: t.nishizawa@riam.kyushu-u.ac.jp

In the region where q is near zero, the field lines are oriented mostly in the poloidal direction. In addition, this q profile leads to much greater normalized magnetic shear $\hat{s} \equiv (r/q)\mathrm{d}q/\mathrm{d}r$ compared with that of tokamaks or stellarators. Due to these features, unexplored parameter regimes can be investigated by using PPCD. In this article, theoretical and experimental studies of micro-instabilities in PPCD are reviewed.

5.2 Identification of dominant instabilities through linear analyses

Using the gyrokinetic turbulence code GENE [5, 6], linear stability analyses of micro-instabilities in RFP plasmas with PPCD have been performed for experimentally observed profiles in the MST RFP [7, 8]. Fig. 2 shows the linear growth rates and frequencies for different radial locations. At low toroidal wavenumbers k_y and for most radii, the unstable drift waves propagate in the electron diamagnetic direction and are identified as trapped-electron modes (TEMs) through the cross-phases between the fluctuations of the electrostatic potential and the density of the passing vs. trapped electrons, as well as through sensitivity scans over density and temperature gradients.

The scan of $\eta \equiv (\mathrm{d}\ln T/\mathrm{d}r)/(\mathrm{d}\ln n/\mathrm{d}r)$ demonstrates that the dominant instability transitions to the ion temperature gradient (ITG) mode when η is raised to 1.5. Note $\eta_\mathrm{i} = \eta_\mathrm{e}$ for the profiles investigated. While experimental

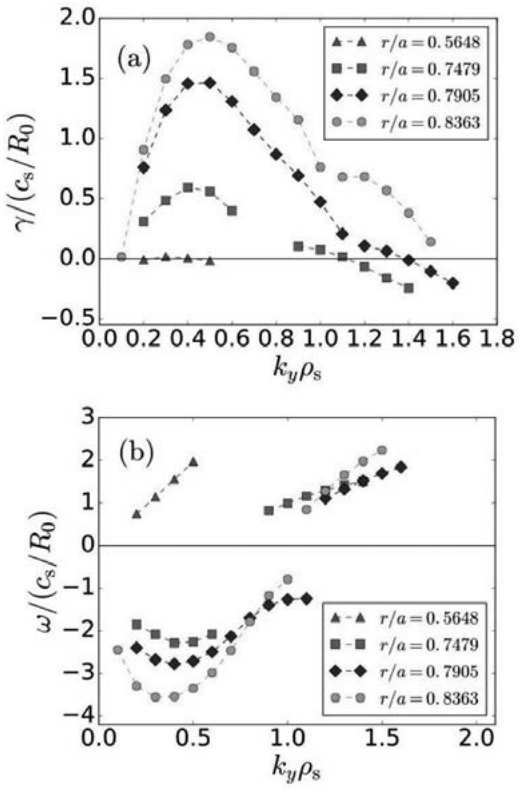

Fig. 2 Linear analysis of a low-η RFP discharge with PPCD. Linear growth rates (a) and real frequencies (b) are shown as a function of a normalized toroidal wavenumber $k_y\rho_s$, respectively, with negative frequencies corresponding to the electron diamagnetic drift direction. r/a is the radial position normalized by the plasma minor radius and ρ_s is the ion sound gyroradius.

investigations of ITG turbulence in RFPs are still lacking, a reactor-relevant RFP requires higher η and may operate in an ITG-dominated regime.

5.3 Nonlinear dynamics of drift-wave turbulence in RFPs

The nonlinear evolution of turbulence in this RFP PPCD scenario has also been investigated in Ref. [7]. Fig. 3(a) shows a snapshot of the electric potential in the x-y (radial-toroidal) plane. In this simulation, tearing modes are ignored, and the magnetic configuration is purely axisymmetric. The electric potential has a laminar structure with $k_x = 0$ and without eddies, showing that zonal flows [9] develop to large amplitudes and suppress turbulence. These pronounced zonal flows are in large part due to a sizable zonal-flow residual [10], which is a measure of how resilient zonal flows are to decay based on linear physics. The zonal flow residual in axisymmetric systems is given by

$$\frac{\Phi_\mathrm{res}}{\Phi_0} = \frac{1}{1 + 1.6q^2/\epsilon_\mathrm{t}^{1/2}}, \tag{1}$$

where Φ_0 is the initial amplitude of the electrostatic potential, and ϵ_t is the inverse aspect ratio of the flux surface. Since q is at least one order of magnitude smaller than in tokamaks, RFP plasmas have significantly higher zonal-flow residuals and can more effectively sustain zonal flows.

However, the inferred electron heat transport level in these nonlinear simulations is much lower than what is observed experimentally, indicating that other physics critically affect outcomes. In experiments, the degree of PPCD-based tearing-mode suppression varies with mode number. Even in the most successful PPCD discharges, there remain finite global-scale magnetic fluctuations originating from residual tearing activity. When these residual global-scale magnetic fluctuations are modeled by an ad-hoc, constant-in-time perturbation in gyrokinetic simulations [7], fully-developed TEM turbulence as shown in Fig. 3(b) is obtained. The resulting electron heat transport in this case falls within the range expected from the experiments. For an ITG-dominated regime, the difference in turbulence and transport in the presence or absence of the ad-hoc perturbation is less striking. In Fig. 4, the electron heat fluxes with and without residual magnetic fluctuations are shown for both TEM and ITG cases. In the ITG-dominated scenario, an experimentally relevant heat flux is still driven without added magnetic perturbation. In addition, the increase in the heat flux by incorporating the residual tearing modes is modest compared with the TEM case.

The difference between the nonlinear simulations with and without the ad-hoc perturbation in the TEM and ITG cases can be understood through the dominant mechanisms of turbulence saturation. In addition to turbulence decorrelation by sheared flows, mode coupling to stable modes mediated by marginally stable eigenmodes can also regulate the development of turbulence [11]. The ITG turbulence obtained in the RFP geometry is identified to be of the slab-ITG type. Unlike the toroidal ITG, which is typically more relevant in tokamaks, and for which zonal flows effectively regulate turbulence, saturation of the slab ITG

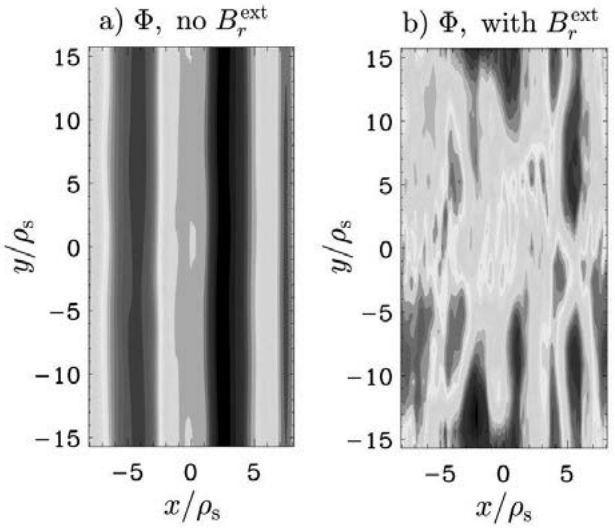

Fig. 3 Electrostatic potential contours (in units of $\rho_s e/(R_0 T_e)$) in TEM turbulence for simulations with zero (a) and finite (b) residual magnetic tearing fluctuations. Here, e is the elementary charge and R_0 is the major radius of the magnetic axis. The horizontal and vertical directions correspond to the radial and toroidal directions, respectively.

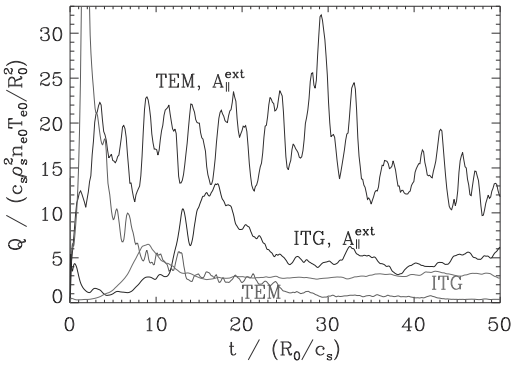

Fig. 4 Electrostatic electron heat flux time traces, with (black and blue) and without (red and magenta) a magnetic perturbation modeling tearing modes. TEM transport (black and red) is increased by orders of magnitude, while ITG transport (blue and magenta) only changes by approximately a factor of two, despite imposing an identical tearing perturbation.

relies less prominently on zonal flows. Thus, the electron heat flux is less affected by the generation and disruption of zonal flows in the ITG case.

The same type of externally imposed resonant magnetic fluctuation has been used in a study of edge turbulence in the tokamak L-mode [12], successfully recovering trends from experimental beam-emission-spectroscopy measurements. There, the turbulence is driven by a mixture of toroidal ITG modes and TEMs. Its response to increasing external perturbation is more complex: fluxes first increase as zonal flows begin to be eroded, before decreasing again as the width of the imposed island—note that the perturbation causes only partial stochastization—reaches the typical scale of radial temperature corrugations. At that point, the tertiary drive of the instability is reduced, and fluxes begin to fall, before zonal-flow erosion once more becomes dominant, and fluxes rise again. While illustrating interesting physics possibly exploitable in designing perturbative coils for the suppression of edge-localized modes, it also raises the question to what degree this ad-hoc perturbation is truly reflective of the situation in the RFP, where larger-scale islands, a larger degree of stochastization, and the possible feedback of the turbulence on the tearing modes may need to be taken into account.

More recently, the GENE code has been upgraded to incorporate a background current gradient via shifted Maxwellian equilibrium distribution functions, thus allowing for the linear and nonlinear study of tearing modes in RFPs and tokamaks [13]. This technology has since been deployed to numerically evaluate the cross-scale interaction between tearing modes and microturbulence in the RFP self-consistently [14]. While only resolving a sparse spectrum (multiples of toroidal mode number $n = 5$), leading to a lower tearing fluctuation level and stochastization, this work confirms that the physics of zonal-flow erosion modeled in the earlier work with the ad-hoc perturbation are indeed at play, while no strong back-reaction of the microturbulence on the low-n tearing modes is seen due to the radial separation. Notably, zonal-flow erosion relies on low-n core tearing modes first coupling to excite linearly stable, higher-n edge tearing modes nonlinearly, which then interact with the TEM turbulence in the edge.

5.4 Experimental investigation of microturbulence in RFP

At the MST RFP, high frequency fluctuations around 100 kHz have been observed when tearing modes are reduced by PPCD. Fig. 5 shows spectrograms of the electron density and C III emission intensity fluctuations, as well as the amplitude of magnetic fluctuations at the wall. PPCD is applied at 10 ms, and the period with reduced magnetic fluctuations lasts until around 22.5 ms. Using the two-point correlation technique, the peak of the wavenumber spectrum of this mode is measured to be around 0.5 cm^{-1}, which is on the scale of the ion gyro-radius [15]. In addition, simultaneous measurements of the perpendicular C^{2+} flow and the emission intensity fluctuations of C III confirmed that this mode propagates in the electron diamagnetic drift direction [15]. At a lower plasma current, with which successful reduction of tearing-mode fluctuations is more reliably achieved, multi-chord interferometer measurements have shown that the high-frequency fluctuations appear only when the density gradient in the edge exceeds a certain threshold [16]. These observations are consistent with density-gradient-driven TEM turbulence, which is predicted to be unstable in these discharges based on linear gyrokinetic analyses.

The impurity particle flux associated with the high-frequency fluctuations (∼100 kHz) shown in Fig. 5 is also directly evaluated by using ion-Doppler spectroscopy [17]. For this measurement, a spectrometer with high throughput and wavelength resolution and a new correlation analysis technique has been developed to resolve the radial velocity fluctuations [18, 19]. As shown in Fig. 6, substantial flux of C^{2+} exists around 100 kHz. This fluctuation-driven flux is comparable with the total C^{2+} flux estimated from the radial distribution of carbon impurities and their ion-

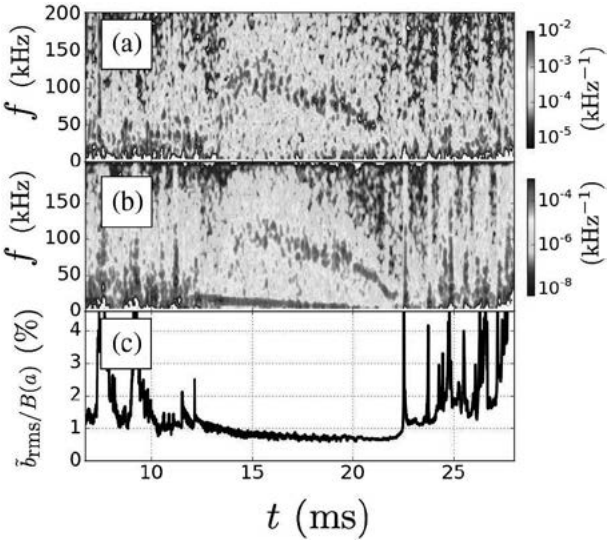

Fig. 5 (a) Spectrogram of normalized C III 464.7 nm emission intensity fluctuations. (b) Spectrogram of normalized chord-integrated electron density intensity fluctuations at impact parameter $R - R_0 = 43$ cm ($r/a = 0.86$). (c) Tangential component of normalized magnetic fluctuations at $r = a$. Figure reprinted from Ref. [17] with permission, copyright 2018 by the American Physical Society.

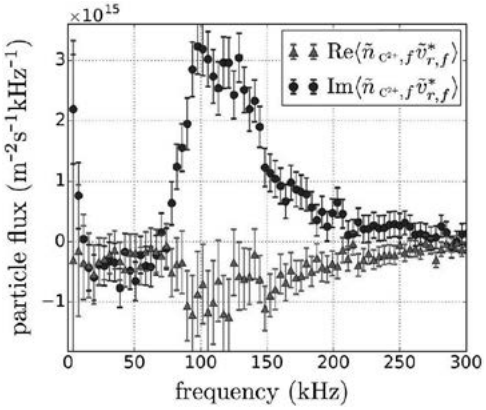

Fig. 6 Spectral density of the impurity particle flux (red triangles) and the circulating flow (blue circles) due to microturbulence. Figure reprinted from Ref. [17] with permission, copyright 2018 by the American Physical Society.

ization and recombination rates [20]. This result provides experimental evidence that micro-instabilities can become a dominant transport channel in the RFP.

5.5 Zonal flows in the RFP

The gyrokinetic simulations have demonstrated that zonal flows govern the amplitude of TEM turbulence and the resulting transport. To confirm that zonal flows are actually at play in real RFP plasmas, an experimental investigation of zonal flows has been performed. Zonal flows have the mode structure of $m = n = 0$, and their radial wavelengths are on the order of a few ion gyro-radii [21]. To search for these characteristics, the radial electric field E_r is measured at two both poloidally and toroidally separated locations by using multichannel capacitive probes [22, 23].

Fig. 7(a) shows the radial profile of the power spectral

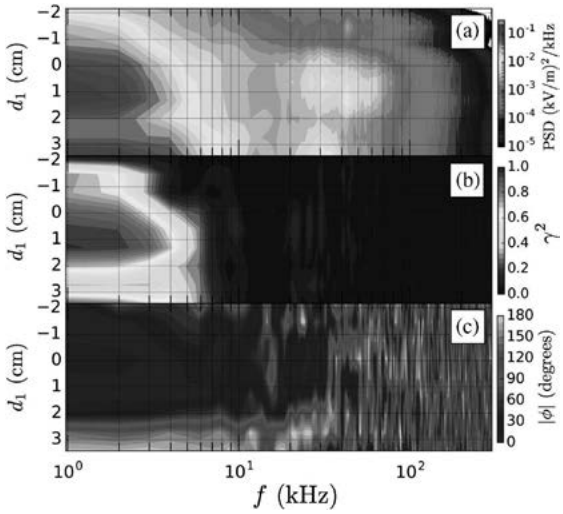

Fig. 7 (a) Profile of the power spectral density (PSD) of the perturbed E_r in the location of the first probe. Coherence (b) and cross phase (c) between E_r at the minimum of the E_r well in the second probe location and E_r in the first probe location. d_1 represents the distance from the LCFS, and $d_1 > 0$ is in the confinement region. Figure reprinted from Ref. [22] with permission, copyright 2019 by the American Physical Society.

density of the E_r fluctuations during the PPCD period. The mean radial E_r profile has a well structure just inside the last closed flux surface (LCFS). The amplitude of the low-frequency components (<10 kHz) of the E_r fluctuations peaks near 1 cm from the LCFS and decreases as the radial location moves further into the core. However, the fluctuation amplitude increases again for $d_1 > 2$ cm. By using the time evolution of E_r at the minimum of the E_r well measured by the second probe as reference, long-range correlations of E_r fluctuations are evaluated for each radial location. Coherence with respect to the E_r at the second probe's reference channel is shown in Fig. 7(b). The coherence in the low frequencies is high at $d_1 \sim 1$ cm, which corresponds to the minimum of the E_r well at the location of the first probe. Interestingly, high coherence is also obtained for $d_1 > 3$ cm. Since the ion gyro-radius in these radial locations is ≈1 cm, this coherence profile shows that the radial structure of low-frequency fluctuations varies on the order of the ion gyro-radius. The phase angles of the coherence shown in Fig. 7(b) are plotted in Fig. 7(c). At the minimum of the E_r well, the low-frequency fluctuations are in phase, satisfying the expectations of the $m = n = 0$ mode structure. On the other hand, the phase angle becomes ∼180° at $d_1 = 3.5$ cm, and the fluctuation here is out of phase with respect to the minimum of the E_r well. Thus, the $E \times B$ flow associated with E_r changes its direction around $d_1 = 2.5$ cm, and these counterflows are synchronized. This observation is consistent with the situation in which two layers of zonal flows exist just inside the LCFS.

The observation of zonal flows near the plasma boundary has implications for the mechanism of the L-H transition in tokamaks, the details of which still remain an active field of research [24]. Some experimentally observed L-H transitions can be explained by a predator-prey (PP)

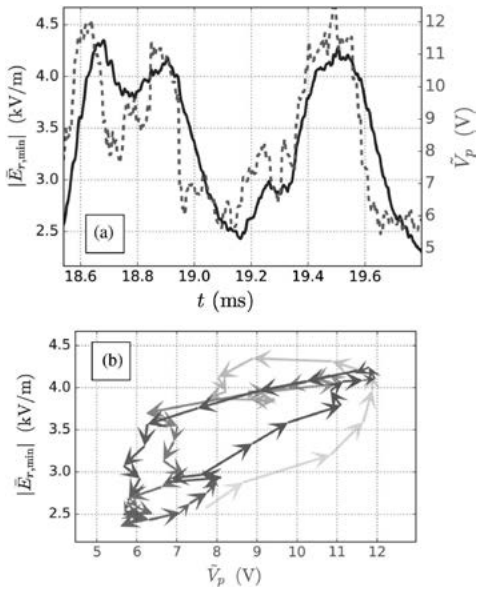

Fig. 8 (a) Time evolution of the depth of the E_r well and the root-mean-square of the plasma potential fluctuation above 20 kHz. (b) The corresponding Lissajous curve: each arrow represents a time step of 50 μs. Figure reprinted from Ref. [22] with permission, copyright 2019 by the American Physical Society.

model [25, 26] in which zonal flows initially suppress turbulence and facilitate the formation of a transport barrier sustained by the ion pressure gradient. However, zonal flows are not necessarily always observed at the onset of L-H transition [27, 28], and the validity of the PP model has been debated for a number of years. While an L-H transition has not been observed in RFPs so far, the E_r measurements at MST strongly suggest that zonal flows can exist just inside the LCFS of a toroidal plasma where an edge transport barrier forms during the L-H transition of tokamaks. In the PP model, a limit cycle oscillation (LCO) is expected between the amplitudes of turbulence and a zonal flow. As shown in Fig. 8, an LCO is also observed in the MST RFP between the depth of the E_r well and the amplitude of the potential fluctuations.

5.6 Summary

Due to the unique magnetic configuration, RFPs are able to probe the physics of plasma micro-instabilities by reaching parameter regimes which cannot be accessed by tokamaks or stellarators. Based on gyrokinetic simulations in a local flux tube and ignoring tearing modes, a pure axisymmetric RFP configuration leads to unphysically low transport levels due to zonal flows with extremely high amplitudes when the TEM is the dominant instability. By imposing ad-hoc, constant-in-time magnetic perturbations in these simulations, which arise from residual tearing modes in real experiments, the zonal flows are disrupted, and realistic transport levels are obtained. These mechanisms have since been confirmed through self-consistent multi-scale global gyrokinetic simulations. In contrast, slab ITG turbulence can develop without such magnetic perturbations since the nonlinear saturation in this case does not as strongly rely on zonal flows.

Experimentally, characteristics consistent with TEM turbulence are obtained through fluctuation measurements of multiple plasma parameters at the MST RFP. In addition, a micro-instability is shown to drive a significant impurity flux, and zonal flows are also observed.

Due to the small number of RFP experiments in the world – and particularly that of RFPs with high-performance, tearing-suppressed operation – the literature on microinstability and microturbulence in RFP plasmas is strongly limited. At the same time, studies of such turbulence in the RFP have revealed rich, multi-scale physics and have helped uncover processes of direct relevance to other magnetic confinement device classes. Furthermore, the propensity of RFPs for effectively sustaining zonal flows may, if tearing-based zonal-flow erosion can be avoided or otherwise mitigated, make the RFP a highly desirable configuration able to sustain high pressure gradients. Paired with the lower capital cost of RFPs, this may indeed make this type of fusion reactor a strong contender for commercialization.

Acknowledgments

We thank Z. R. Williams and P. W. Terry for their contributions to the theoretical analysis and simulations, and the MST team for their experimental support.

References

[1] D.J. Thuecks *et al.*, Phys. Plasmas **24**, 022309 (2017).
[2] J.S. Sarff, in this special topic.
[3] L. Marrelli, in this special topic.
[4] M. Zuin *et al.*, Phys. Rev. Lett. **110**, 055002 (2013).
[5] F. Jenko *et al.*, Phys. Plasmas **7**, 1904 (2000).
[6] https://www.genecode.org/
[7] Z.R. Williams *et al.*, Phys. Plasmas **24**, 122309 (2017).
[8] D. Carmody *et al.*, Phys. Plasmas **22**, 012504 (2015).
[9] P.H. Diamond *et al.*, Plasma Phys. Control. Fusion **47**, R35 (2005).
[10] H. Sugama and T.-H. Watanabe, Phys. Plasmas **13**, 012501 (2006).
[11] P.W. Terry *et al.*, Phys. Plasmas **16**, 122305 (2009).
[12] Z.R. Williams *et al.*, Nucl. Fusion **60**, 096004 (2020).
[13] T. Jitsuk *et al.*, Nucl. Fusion **64**, 046005 (2024).
[14] T. Jitsuk *et al.*, Phys. Rev. Lett. **136**, 015101 (2026).
[15] T. Nishizawa, Ph.D. thesis, University of Wisconsin-Madison (2018).
[16] J.R. Duff *et al.*, Phys. Plasmas **25**, 010701 (2018).
[17] T. Nishizawa *et al.*, Phys. Rev. Lett. **121**, 165002 (2018).
[18] D. Craig *et al.*, Rev. Sci. Instrum. **78**, 013103 (2007).
[19] T. Nishizawa *et al.*, Rev. Sci. Instrum. **88**, 083513 (2017).
[20] T. Barbui *et al.*, Plasma Phys. Control. Fusion **56**, 075012 (2014).
[21] A. Fujisawa *et al.*, Phys. Rev. Lett. **93**, 165002 (2004).
[22] T. Nishizawa *et al.*, Phys. Rev. Lett. **122**, 105001 (2019).
[23] T. Nishizawa *et al.*, Rev. Sci. Instrum. **89**, 10J118 (2018).
[24] T. Kobayashi, Nucl. Fusion **60**, 095001 (2020).
[25] E. Kim and P.H. Diamond, Phys. Rev. Lett. **90**, 185006 (2003).
[26] L. Schmitz *et al.*, Phys. Rev. Lett. **108**, 155002 (2012).
[27] T. Kobayashi *et al.*, Phys. Rev. Lett. **111**, 035002 (2013).
[28] M. Cavedon *et al.*, Nucl. Fusion **57**, 014002 (2016).